Systematic error in the estimation of the second order moments of wind speeds by lidars

Sathe, A.; Mann, Jakob; Gottschall, Julia; Courtney, Michael

Published in:
Detailed Program (online)

Publication date:
2010

Document Version
Publisher's PDF, also known as Version of record

Systematic error in the estimation of the second order moments of wind speeds by lidars

A. SATHE[1], J. MANN[2], J. GOTTSCHALL[2], M. S. COURTNEY[2]

[1] *L& R, Section Wind Energy, TU Delft, Kluyverweg 1, 2629 HS Delft, The Netherlands. E-mail: A.R.Sathe@tudelft.nl*

[2] *Wind Energy Division, Risø DTU, Frederiksborgvej 399, 4000 Roskilde, Denmark*

1 INTRODUCTION

A theoretical model is developed to estimate the systematic errors in the second-order moments of wind speeds measured by lidars. The systematic errors are the errors that arise due to the averaging effect in the line-of-sight and the quite large circle in which lidars measure wind speed. Two types of lidars are considered, the ZephIR developed by QinetiQ (Natural Power) as a continuous wave (CW) lidar and the WindCube developed by Leosphere as a pulsed lidar. The verification is carried out by comparing the second order moments measured by ZephIR and WindCube with that of the sonic anemometer placed at different heights on a meteorological mast.

One of the first turbulence studies by lidars was carried out by [1], which was more a demonstration of feasibility of turbulence measurements by lidars since no measurements were available high up in the atmospheric boundary layer for comparison. [2] presented a technique to analyse lidar data for turbulence measurements, which was done mainly beyond $600\ \mathrm{m}$ due to coarse spatial resolution. [3] presented a detailed analysis of estimating the random errors in the measurement of the mean wind speed by lidars using the theory of isotropic turbulence. [4] demonstrated the sensitivity of the streamwise velocity variance to the spatial and temporal averaging. [5] presented a method to use lidar data for the estimation of turbulent energy dissipation rate from the point of view of studying wake vortices from an aircraft. A comprehensive review is given in [6] that covers different remote sensing techniques for turbulence measurements including lidars. A review of the use of lidars for wind energy applications is also presented in [7]. Recently, studies have been carried out to model the spatial averaging effects [8] and compare the 3D turbulence measurements using three staring lidars [9]. [10] modelled the systematic errors by approximating the conical scan as a length scale. [11] attempted to estimate the momentum fluxes using lidars and model the unfiltered turbulence from the CW lidar. In this work averaging effects due to the full extent of conical scanning and line-of-sight averaging is considered.

2 THEORY

The model in this work is developed for the velocity azimuth display (VAD) technique of lidar scanning. The line-of-sight velocity (also called as radial velocity v_r) is measured by the lidar at each azimuth angle θ. The half cone opening angle ϕ is kept constant throughout the scan. The CW and pulsed lidars work on the principle of backscattering of the emitted radiation and subsequent detection of the Doppler shift in the frequency of the emitted radiation. Mathematically, v_r is given as the dot product of the unit directional vector and the velocity field at the point of focus,

$$v_r(\theta) = \boldsymbol{n}(\theta) \cdot \mathbf{v}(d_f \boldsymbol{n}(\theta)) \tag{1}$$

where d_f is the focus distance at which the wind speeds are measured, $\mathbf{v} = (u, v, w)$ is the velocity field evaluated at the focus point $d_f\boldsymbol{n}(\theta)$ and $\boldsymbol{n}(\theta)$ is the unit directional vector given as,

$$\boldsymbol{n}(\theta) = (\cos\theta \sin\phi, \sin\theta \sin\phi, \cos\phi) \tag{2}$$

In reality it is impossible to obtain the backscattered radiation precisely from only the focus point and there is always backscattered radiation of different intensities from different regions in space along the line-of-sight. Hence, it is necessary to assign appropriate weights to the backscattered intensity such that the weight corresponding to the focus point is the highest. Mathematically the weighted average radial velocity can be written as,

$$\tilde{v}_r(\theta) = \int_{-\infty}^{\infty} \varphi(s) \boldsymbol{n}(\theta) \cdot \mathbf{v}(s\boldsymbol{n}(\theta) + d_f \boldsymbol{n}(\theta))\, ds \tag{3}$$

where $\varphi(s)$ is any weighting function and s is the the distance from the focus. For simplicity we assume that $s = 0$ corresponds to the focus distance. Our model is based on the assumptions of homogeneity and neutral atmospheric conditions. The flow field is also assumed to be frozen during one scan revolution. It is further assumed that Eq. 3 with an appropriately chosen $\varphi(s)$ models the averaging well.

2.1 Systematic Error in CW lidar

The CW lidar scans at many points on the azimuth circle. For the ZephIR lidar considered in our case a typical scan consists of measurements of v_r at 50 points on the azimuth circle, and often three circles are used to get a single velocity vector. If we assume that u is aligned to the mean wind direction, v is perpendicular to the mean wind direction, w lies on the vertical axis and the mean wind comes from the North then $\tilde{v_r}(\theta)$ can be expressed as,

$$\tilde{v_r}(\theta) = A + B\cos\theta + C\sin\theta \tag{4}$$

where the coefficients $A = w\ \cos\phi$, $B = u\ \sin\phi$ and $C = v\ \sin\phi$ and the sign ambiguity in $\tilde{v_r}(\theta)$ is neglected. The assumption that the mean wind comes from the North is only made for simplicity. For a lidar measuring at many points on the azimuth circle the choice of the mean wind direction does not matter since averaging over the entire circle is carried out. The values of the coefficients A, B and C are found using least squares method by fitting the measured values of $\tilde{v}_r(\theta)$ at several azimuth angles in Eq. (4). Thus the coefficients can be written as Fourier integrals,

$$A = \frac{1}{2\pi}\int_0^{2\pi} \tilde{v}_r(\theta)\ d\theta \tag{5a}$$

$$B = \frac{1}{\pi}\int_0^{2\pi} \tilde{v}_r(\theta)\ \cos\theta\ d\theta \tag{5b}$$

$$C = \frac{1}{\pi}\int_0^{2\pi} \tilde{v}_r(\theta)\ \sin\theta\ d\theta \tag{5c}$$

The variance of any variable X can be denoted as $\sigma_X^2 = \langle X'^2\rangle$, where $\langle\rangle$ denotes ensemble averaging. Applying this definition to coefficients A, B and C (Eqs. 5a–5c) and using Eq. (3), the following expressions are derived:

$$\langle w'^2\rangle \cos^2\phi = \int \Phi_{ij}(\boldsymbol{k})\alpha_i(\boldsymbol{k})\alpha_j^*(\boldsymbol{k})\ d\boldsymbol{k} \tag{6}$$

$$\langle u'^2\rangle \sin^2\phi = \int \Phi_{ij}(\boldsymbol{k})\beta_i(\boldsymbol{k})\beta_j^*(\boldsymbol{k})\ d\boldsymbol{k} \tag{7}$$

$$\langle v'^2\rangle \sin^2\phi = \int \Phi_{ij}(\boldsymbol{k})\gamma_i(\boldsymbol{k})\gamma_j^*(\boldsymbol{k})\ d\boldsymbol{k} \tag{8}$$

$$\langle u'w'\rangle \sin\phi\cos\phi = \int \Phi_{ij}(\boldsymbol{k})\beta_i(\boldsymbol{k})\alpha_j^*(\boldsymbol{k})\ d\boldsymbol{k} \tag{9}$$

where $\langle u'^2\rangle$, $\langle v'^2\rangle$, $\langle w'^2\rangle$ are the variances of the u, v and w velocity respectively, $\langle u'w'\rangle$ is the momentum flux, $\Phi_{ij}(\boldsymbol{k})$ is the three dimensional spectral velocity tensor, $\boldsymbol{k} = (k_1, k_2, k_3)$ is the wave vector, $*$ denotes complex conjugation and α_i, β_i and γ_i are the weighting functions given as,

$$\alpha_i(\boldsymbol{k}) = \frac{1}{2\pi}\, e^{\mathrm{i}d_f k_3\cos\phi} \int_0^{2\pi} n_i(\theta+\theta_0)\, e^{\mathrm{i}d_f k_h \sin\phi\cos\theta}\, e^{-l|k_h\sin\phi + k_3\cos\phi|}\ d\theta \tag{10}$$

$$\beta_i(\boldsymbol{k}) = \frac{1}{\pi}\, e^{\mathrm{i}d_f k_3\cos\phi} \int_0^{2\pi} n_i(\theta+\theta_0)\cos(\theta+\theta_0)\, e^{\mathrm{i}d_f k_h \sin\phi\cos\theta}\, e^{-l|k_h\sin\phi + k_3\cos\phi|}\ d\theta \tag{11}$$

$$\gamma_i(\boldsymbol{k}) = \frac{1}{\pi}\, e^{\mathrm{i}d_f k_3\cos\phi} \int_0^{2\pi} n_i(\theta+\theta_0)\sin(\theta+\theta_0)\, e^{\mathrm{i}d_f k_h \sin\phi\cos\theta}\, e^{-l|k_h\sin\phi + k_3\cos\phi|}\ d\theta \tag{12}$$

where $k_h = \sqrt{k_1^2 + k_2^2}$ is the magnitude of the horizontal wavenumber vector, $\cos\theta_0 = k_1/k_h$, $\sin\theta_0 = k_2/k_h$, and $n_i(\theta+\theta_0)$ is the component of the unit directional vector obtained from Eq. 2. The analytical expressions for $\Phi_{ij}(\boldsymbol{k})$ are used from [12]. Eqs. (10–12) are numerically integrated along with $\Phi_{ij}(\boldsymbol{k})$ (Eqs. 6–9) to estimate the second-order moments measured by CW lidars.

2.2 Systematic Error in pulsed lidars

The assumption made in section 2.1 that the mean wind direction comes from the North cannot be made for WindCube since it measures at four azimuth angles only, viz. North (N), East (E), South (S), West (W). In this case the coordinate system is such that u is aligned in the mean wind direction. Then u and v are given as,

$$u = u_{NS}\cos\Theta + u_{EW}\sin\Theta \tag{13}$$

$$v = u_{NS}\sin\Theta - u_{EW}\cos\Theta \tag{14}$$

where u_{NS} and u_{EW} denote wind speeds in the North-South and East-West directions respectively

and Θ denotes the wind direction. From simple geometrical considerations we can also write,

$$u_{NS} = \frac{\tilde{v}_{rN} - \tilde{v}_{rS}}{2\sin\phi} \quad (15)$$

$$u_{EW} = \frac{\tilde{v}_{rE} - \tilde{v}_{rW}}{2\sin\phi} \quad (16)$$

$$w = \frac{\tilde{v}_{rN} + \tilde{v}_{rS} + \tilde{v}_{rE} + \tilde{v}_{rW}}{4\cos\phi}, \quad (17)$$

where $\tilde{v}_{rN}$, $\tilde{v}_{rS}$, $\tilde{v}_{rE}$, $\tilde{v}_{rW}$ represent the weighted average radial velocities in the North, South, East and West directions respectively. Proceeding in a similar manner as in section 2.1, we get expressions for the second order moments in terms of the weighting functions $a_i(\boldsymbol{k})$, $b_i(\boldsymbol{k})$ and $c_i(\boldsymbol{k})$ for w, u and v respectively. b_i is given as,

$$\begin{aligned} b_i(\boldsymbol{k}) = & \frac{1}{2\sin\phi}[(n_{iN}e^{\mathrm{i}d_f\boldsymbol{k}\cdot\boldsymbol{n_N}}\hat{\varphi}(\boldsymbol{k}\cdot\boldsymbol{n_N}) \\ & - n_{iS}e^{\mathrm{i}d_f\boldsymbol{k}\cdot\boldsymbol{n_S}}\hat{\varphi}(\boldsymbol{k}\cdot\boldsymbol{n_S}))\cos\Theta \\ & + (n_{iE}e^{\mathrm{i}d_f\boldsymbol{k}\cdot\boldsymbol{n_E}}\hat{\varphi}(\boldsymbol{k}\cdot\boldsymbol{n_E}) \\ & - n_{iW}e^{\mathrm{i}d_f\boldsymbol{k}\cdot\boldsymbol{n_W}}\hat{\varphi}(\boldsymbol{k}\cdot\boldsymbol{n_W}))\sin\Theta] \end{aligned} \quad (18)$$

where $\hat{}$ denotes Fourier transform. It is worth noting from Eq. (18) that $b_i(\boldsymbol{k})$ depends on Θ. The expressions for $a_i(\boldsymbol{k})$ and $c_i(\boldsymbol{k})$ are very similar to Eq. (18) except that the variation with wind direction for $c_i(\boldsymbol{k})$ is deduced from Eq. (14). $a_i(\boldsymbol{k})$ does not vary with Θ as seen from Eq. (17).

3 DATASETS

The measurements are carried out at Høvsøre, which is the national wind turbine test center in Denmark. At this site five wind turbines are placed to the North of the met-mast (coordinates $56°26'26"$ N, $08°09'03"$ E). 20 Hz sonic measurements are used to compute true second order moments. They are mounted on booms in the North direction. The ZephIR and WindCube take approximately 1 and 6 s respectively to complete one scan in the VAD technique. They are placed at about 40 and 15 m to the North and West of the met-mast respectively. The half cone opening angle for both lidars is $30°$. To ensure that the wake effects from the wind turbines and met-mast do not influence the measurements, the wind direction sector that is chosen for the analysis is $230°$–$300°$. Since the systematic error in the lidar turbulence measurements changes with height, four heights were chosen, viz. 40, 60, 80 and 100 m. The period of analysis is between January 2009 and November 2009. The wind speeds between 4 and 25 m/s only are used. The data are also filtered for periods of rain.

4 COMPARISON WITH MEASUREMENTS

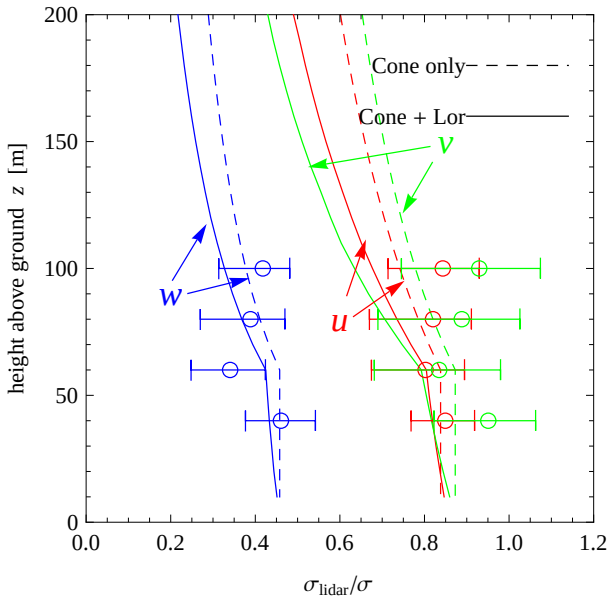

Figure 1: Comparison of the systematic error by ZephIR. The dotted line shows only cone averaging and the solid line shows the averaging due to cone and φ, assumed Lorentzian

Figure 1 shows the comparison of the systematic error of the second order moments in the CW lidar (ZephIR) modelled in section 2.1 with the measurements. The model shows that the systematic error increases (i. e. the ratio of the second order moment measured by CW lidar to the true second order moment decreases) with height for u, v and w. This is because the probe length of CW lidar increases quadratically with height and the diameter of the conical circle also increases. The kink at 60 m in the model prediction is because the length scale used in the estimation of Φ_{ij} increases linearly with height up to 60 m and is considered constant beyond. The data shows an increase in the systematic error up to 60 m and a slight reduction beyond. The circles are the medians of the measured ratios of standard deviations while the extremes of the horizontal lines are the 25% and 75% fractiles, respectively. The deviation of the model with the data beyond 60 m could be

because the standard input parameters from [13] from chosen to compute Φ_{ij}. It would be quite interesting to obtain empirical values of the inputs to Φ_{ij} using the measurements at the site as in [14]. Moreover, all atmospheric stability conditions are considered. Both, the model and the data show that the attenuation in w is much larger than in u and v. This can be explained by considering that the length scales for w are much smaller than u and v.

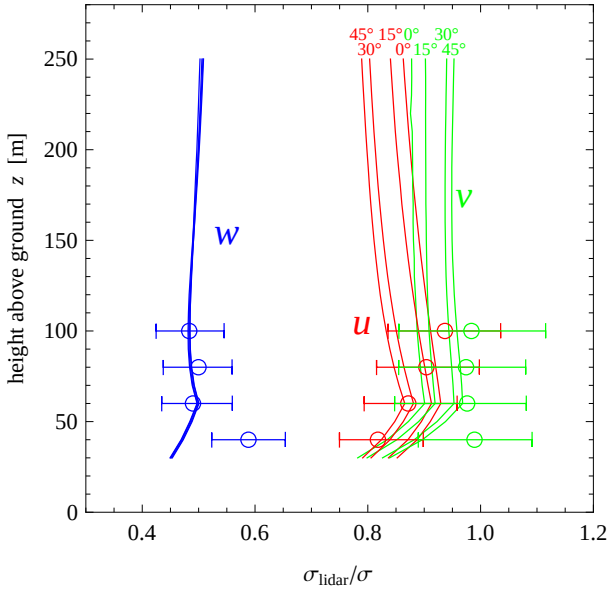

Figure 2: Comparison of the systematic error by WindCube. Variation with wind direction is also seen.

Figure 2 shows the comparison of the systematic error of the second order moments in the pulsed lidar (WindCube) modelled in section 2.2 with the measurements. WindCube has a constant probe length, and hence, the model shows that the systematic error decreases with height. Beyond 60 m the model predicts a slight increase in the systematic error with height. This is because the attenuation due to the circle averaging is more dominant than the attenuation due to the probe length. The dependence of the systematic error on the wind direction is also seen. The data shows a good agreement with the model for w at 60, 80 and 100 m. For u there is an increase in the systematic errors at all heights, whereas for v there is a slight increase up to 60 m and a decrease beyond.

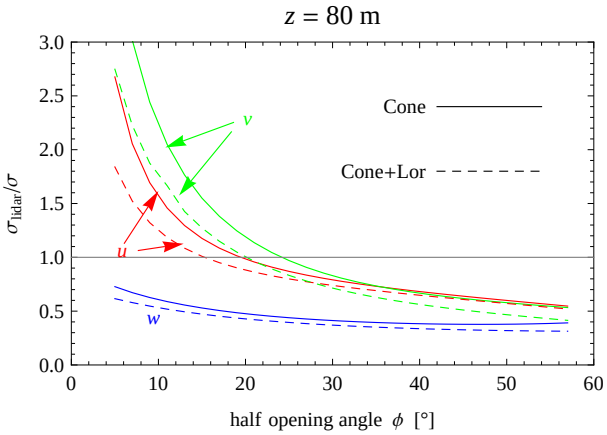

Figure 3: The sensitivity of the systematic errors to ϕ at $z = 80$ m. The solid line shows only cone averaging and the dotted line shows the averaging due to cone and φ, where φ is modelled using Lorentzian

Figure 3 shows the variation of the systematic error with respect to ϕ. It decreases non-linearly with ϕ. The influence of line-of-sight averaging (Lorentzian) is not considerable.

5 CONCLUSION AND DISCUSSION

Systematic error in the second order moments is modelled for the CW and pulsed lidar. In general the systematic error increases with increasing height for the CW lidar, whereas it decreases with increasing height for the pulsed lidar. The model agrees well with the data for WindCube for u and w. Owing to the smaller length scales for w the systematic error is quite large in comparison to u and v. Further investigation will focus on estimating the inputs to Φ_{ij} empirically. The data will be separated into different stability classes and a comparison will be made with the model.

References

[1] W L. Eberhard, R E. Cupp, and K R. Healy. Doppler lidar measurements of profiles of turbulence and momentum flux. *Journal of Atmospheric and Oceanic Technology*, 6:809–819, 1989.

[2] T. Gal-Chen, M. Xu, and W L. Eberhard. Estimation of atmospheric boundary layer fluxes

and other turbulence parameters from Doppler lidar data. *Journal of Geophysical Research*, 97(D17):18,409–18,423, 1992.

[3] V A. Banakh, I N. Smalikho, F. Köpp, and C. Werner. Representativeness of wind measurements with a CW Doppler lidar in the atmospheric boundary layer. *Applied optics*, 34(12):2055–2067, 1995.

[4] Y L. Pichugina, R M. Banta, and W A. Brewer. Vertical profiles of velocity variances and TKE using Doppler-lidar scan data. In *17th Symposium on Boundary Layers and Turbulence*, San Diego CA, 2005.

[5] I. Smalikho, F. Kopp, and S. Rahm. Measurement of atmospheric turbulence by 2-μm Doppler lidar. *Journal of Atmospheric and Oceanic Technology*, 22(11):1733–1747, 2005.

[6] D A M. Engelbart, M. Kallistratova, and R. Kouznetsov. Determination of the turbulent fluxes of heat and momentum in the ABL by ground-based remote-sensing techniques (a review). *Meteorologische Zeitschrift*, 16(4):325–335, 2007.

[7] S. Emeis, M. Harris, and R M. Banta. Boundary-layer anemometry by optical remote sensing for wind energy applications. *Meteorologische Zeitschrift*, 16(4):337–347, 2007.

[8] M. Sjöholm, T. Mikkelsen, J. Mann, K. Enevoldsen, and M. Courtney. Spatial averaging-effects on turbulence measured by a continuous-wave coherent lidar. *Meteorologische Zeitschrift*, 18(3, Sp. Iss. SI):281–287, 2009.

[9] J. Mann, J. Cariou, M. Courtney, R. Parmentier, T. Mikkelsen, R. Wagner, P. Lindelow, M. Sjöholm, and K. Enevoldsen. Comparison of 3D turbulence measurements using three staring wind lidars and a sonic anemometer. *Meteorologische Zeitschrift*, 18(2, Sp. Iss. SI):135–140, 2009.

[10] R. Wagner, T. Mikkelsen, and M. Courtney. Investigation of turbulence measurements with a continuous wave, conically scanning lidar. Technical Report Risø-R-1682(EN), Risø DTU, 2009.

[11] J. Mann, A. Peña, F. Bingöl, R. Wagner, and M S. Courtney. Lidar scanning of momentum flux in and above the surface layer. *Journal of Atmospheric and Oceanic Technology*, 2010. DOI:10.1175/2010JTECHA1389.1.

[12] J. Mann. The spatial structure of neutral atmospheric surface-layer turbulence. *Journal of Fluid Mechanics*, 273:141–168, 1994.

[13] IEC. IEC 61400-1. Wind turbines – Design Requirements. 2005.

[14] A. Peña, S-E. Gryning, J. Mann, and C B. Hasager. Length scales of the neutral wind profile over homogeneous terrain. *Journal of Applied Meteorology and Climatology*, 2009.